

**A Generalized Model of Nonlinear Dynamics
in Combined Frequency-Amplitude Modulators**

(Date: 27 February 2009)

G. Consolo¹, V. Puliafito², L. Lopez-Diaz³, F. Nizzoli¹, L. Giovannini¹,
G. Valenti⁴, B. Azzerboni²

¹ Interuniversity Consortium for the Physical Sciences of Matter (CNISM) and Department of Physics, University of Ferrara, Italy

² Department of Matter Physics and Electronic Engineering, University of Messina, Italy

³ Department of Applied Physics, University of Salamanca, Spain

⁴ Department of Sciences for Engineering and Architecture, University of Messina, Italy

ABSTRACT

Research in the area of communications systems, and more in general in the field of information theory, is constantly pursued since new physical mechanisms for the excitation of stable microwave oscillations, such as those based on spin-transfer effects, have been demonstrated to be feasible, demanding in turn for a deeper understanding of the underlying nonlinear dynamics.

Here we formulate a generalized theoretical model to describe the behavior of combined frequency-amplitude modulators whose characteristic parameters exhibit a nonlinear dependence on the input modulating signal. The derived analytical solution may give a satisfactory explanation of recent laboratory observations on magnetic oscillators, indicating that those dynamics cannot be ascribed to a pure frequency modulation process. The model agrees with results of micromagnetic calculations. Because the theory has been developed independently of the mechanism causing the

nonlinearities, it encompasses the description of modulation processes occurring in analog modulators of any physical nature.

PACS: 05.45.-a, 75.30.Ds, 75.40.Mg, 84.30.Qi, 87.75.-d

In communication systems, modulation is the process of varying the characteristic parameters of a periodic high-frequency wave (“carrier”), in accordance with a low-frequency information signal (“modulating”), to obtain a “modulated” signal. The carrier wave is generally a sinusoidal waveform characterized by three modifiable parameters, amplitude, frequency and phase, and the corresponding analog modulation processes are referred to as amplitude modulation (AM), frequency modulation (FM) and phase modulation (PM) respectively¹.

In a classical *linear* FM process, the instantaneous frequency of the output signal undergoes a time variation proportional to the information contained in the input modulating signal. In reality, in addition to the basic type of modulation, other spurious analog modulation processes can take place simultaneously distorting the former^{1,2}.

There exist, however, some real cases in which the input-output characteristic is intrinsically nonlinear³⁻⁶ and the resulting behavior would be that of a *nonlinear* modulator. Such a mechanism is *e.g.* observed in magnetic spin-transfer oscillators⁶⁻¹⁶, where the simultaneous action of a *dc* and an *ac* spin-polarized current may excite a persistent dynamics which was *classified* as a FM output signal⁹. In the cited of experiment in Ref.9, two intriguing features were reported: (i) the frequency of the carrier wave shifts with the increase of the amplitude of the modulating signal; (ii) the spectrum contains sidebands that, even though symmetrically located with respect to the carrier frequency, present different amplitudes. The attempt to justify these dynamics on a physical basis was carried out by both analytical and numerical macrospin models, but without fully succeeding in this goal⁹.

Here we develop a more sophisticated analytical model mainly based on the idea that the nonlinear dependence of both frequency and amplitude of the modulated signal on the information-carrying input signal has to be included⁶. Such approach leads to the development of a generalized model for *combined frequency-amplitude nonlinear* modulators, independently of the physical phenomenon giving rise to the above-cited nonlinearities.

Our benchmark to evaluate the validity of the proposed analytical model is based upon the nonlinear dynamics occurring in magnetic spin-transfer modulators. In particular, considering that the related experimental data⁹ are not accessible, we follow an equivalent procedure where theoretical results are compared with those obtained numerically by using a micromagnetic framework.

Let us denote by $c(t) = A_c \cos(2\pi f_c t)$ the temporal evolution of the *carrier signal* having amplitude A_c and frequency f_c . Because $c(t)$ is a pure sinusoidal wave, it brings no information. On the contrary, we refer to $m(t)$ as the base-band *modulating signal* which carries specifications on the message to be transmitted. Ideally, a FM signal is in the form:

$$s(t) = A_c \cos[\theta_i(t)], \quad (1)$$

where A_c is the constant carrier amplitude and $\theta_i(t)$ is the instantaneous phase of the modulated signal, related to the instantaneous frequency by $f_i(t) = (1/2\pi) d\theta_i(t)/dt$. In a typical FM system, $f_i(t)$ varies *linearly* with the modulating signal $m(t)$ according to:

$$f_i(t) = f_c + k_f m(t), \quad (2)$$

where the parameter k_f is called frequency sensitivity. Integrating eq.(2) with respect to time and multiplying by 2π leads eq.(1) to become:

$$s(t) = A_c \cos \left[2\pi f_c t + 2\pi k_f \int_0^t m(\tau) d\tau \right]. \quad (3)$$

Eq.(3) represents the expression of a FM signal in the time domain. If we consider, for simplicity, $m(t)$ in the form of a sinusoidal wave having amplitude A_m and frequency f_m ,

$$m(t) = A_m \cos(2\pi f_m t), \quad (4)$$

the general expression of a single-tone FM signal becomes:

$$s(t) = A_c \cos[2\pi f_c t + \beta \sin(2\pi f_m t)] \quad (5)$$

where $\beta = k_f A_m / f_m$ is called modulation index. If the message signal $m(t)$ is not a pure tone, as it generally happens in real communications systems, the formulation (5) can be generalized by using a Fourier decomposition by which a generic signal $m(t)$ can be expressed as sum of sinusoidal functions like the one in (4).

The spectrum of the FM signal can be derived by applying the Fourier transform of eq.(5)¹:

$$S(f) = \frac{A_c}{2} \sum_{n=-\infty}^{+\infty} \mathcal{J}_n(\beta) [\delta(f - f_c - nf_m) + \delta(f + f_c + nf_m)] \quad (6)$$

where $\mathcal{J}_n(\beta)$ is the n th-order Bessel function of the first kind and argument β . Because of the linearity existing between $f_i(t)$ and $m(t)$ (see eq.(2)), the spectrum of a classical FM signal contains a central frequency, equal to the carrier frequency, and an infinite set of sidebands (symmetrically located on either sides of the carrier at frequency separations of nf_m) which exhibit a symmetry in amplitude due to the property of the Bessel function $\mathcal{J}_n(\beta) = (-1)^n \mathcal{J}_{-n}(\beta)$.

The modulated signal defined by eq.(3) is a nonlinear function of the modulating signal $m(t)$, which makes FM an intrinsic *nonlinear* modulation process. Nevertheless, because of the linearity given by eq.(2), we might refer to this phenomenon as a *linear* modulation process. In the following, we shall refer to a different situation where the instantaneous frequency depends *nonlinearly* on the modulating signal, such as:

$$f_i(t) = f_c + k_1 m(t) + k_2 m^2(t) + k_3 m^3(t) + k_4 m^4(t) + \dots \quad (7)$$

where now k_h is the h th-order frequency sensitivity coefficient. Here we investigate on the possibility that such nonlinear dependences, like the one shown in eq.(7), may also affect the signal amplitude. In this case, the dependence of the output amplitude on the input signal might be included by generalizing the formulation of the term A_c (defined in eq.(1)) as follows:

$$A_c(t) = \lambda_0 + \lambda_1 m(t) + \lambda_2 m^2(t) + \lambda_3 m^3(t) + \lambda_4 m^4(t) + \dots \quad (8)$$

where λ_k identifies, analogously, k th-order amplitude sensitivity coefficient.

In the field of communications systems, the contemporary validity of eqs. (7) and (8) may be understood by assuming that AM and FM phenomena take place simultaneously. From a more general viewpoint, these assumptions simply describe a non-negligible intrinsic nonlinear dependence of both amplitude and frequency on the input stimulus, as it happens in many real systems (both mechanical³⁻⁵ and magneto-electronic^{6,9-11,16}, to cite a few).

With this in mind, in the following we discuss two theoretical models of nonlinear modulation:

1. “NFM”, which deals with a “pure” FM process where the only hypothesis of nonlinearity made in eq.(7) is included⁹.

2. “NFAM”, which deals with the new formulation of a “combined” FM-AM process where both the hypotheses of nonlinearity made in eqs.(7) and (8) are included.

In particular, it will be shown that, even though the problem is initially tackled in both approaches by assuming FM as the *basic* phenomenon and AM as the *additional* one, the developed models and the corresponding conclusions will be unaffected by such hypothesis.

To illustrate the properties of the “NFM” model, let us assume first the relationship f_i versus m to be represented as a Taylor expansion for small $m(t)$ around f_c , as in eq.(7), and the carrier amplitude A_c to be constant. Substituting the expression (4) into (7), and (7) into (1), after some algebraic steps one ends up with the expression of a *nonlinear* FM output signal:

$$s(t) = A_c \cdot \cos \left[\omega_c^I t + \sum_{h=1}^v \beta_h \sin(h\omega_m t) \right] \quad (9)$$

where v is the order of the polynomial (7), $\omega_m = 2\pi f_m$ is the angular frequency of the modulating signal, β_h represents the h th-order modulation index given by a linear combination of the coefficients k_h , and

$$f_c^I = \frac{\omega_c^I}{2\pi} = \left(f_c + \sum_{h=1}^v \eta_h(k_h) A_m^h \right) \quad (10)$$

represents the central frequency of the modulated signal. In (10), the coefficients $\eta_h(k_h)$ obtained for odd h are identically zero, so that the central frequency f_c^I is shifted, with respect to the frequency of the un-modulated carrier f_c , by an amount which depends on the amplitude of the modulating signal A_m through the coefficients with even index h only. Such a property is the *first* indication of a nonlinear modulation process. In fact, differently from the case of linear modulation,

the central frequency can here undergo either a blue-frequency shift (f_c^I increases with increasing A_m) or a red-frequency shift (f_c^I decreases with increasing A_m) according to the signs of the even coefficients of the Taylor expansion (7).

The Fourier transform of eq.(9) can be approximated as follows:

$$S(f) = \frac{A_c}{2} \sum_{\substack{\zeta_p = -\infty \\ p=1, \dots, v}}^{+\infty} \text{Re} \left\{ \prod_{h=1}^v \mathcal{J}_{\zeta_h}(\beta_h) \right\} \cdot \left[\delta \left(f - f_c^I - f_m \sum_{h=1}^v h \zeta_h \right) + \delta \left(f + f_c^I + f_m \sum_{h=1}^v h \zeta_h \right) \right] \quad (11)$$

It should be mentioned that the arguments of the Bessel functions β_h appearing in (11) might be either positive or negative according to the signs of the coefficients of the Taylor series (see eq.(7)). For negative β_h , the corresponding Bessel function can assume a complex value. However, the modulus of the imaginary part is several orders of magnitude smaller than the one of the real part and can be safely neglected.

According to the “NFM” model (eq.(11)), the frequency spectrum of a nonlinear FM signal consists of a central frequency f_c^I , shifted with respect to the frequency of the un-modulated carrier, and an infinite number of sidebands symmetrically located at $f_c^I \pm l f_m$ (l is the positive integer identifying the sideband order). In this case, however, upper and lower sidebands of l th-order (obtained from (11) under the constrain $\sum_{h=1}^v h \zeta_h = \pm l$) generally exhibit different amplitudes owing to their dependence on the product of Bessel functions of different order. The existence of sidebands symmetrically located with respect to the shifted carrier but asymmetric in amplitude represents the *second* main difference between linear and nonlinear modulation.

To introduce the “NFAM” model, we generalize, according to the hypothesis made in eq.(8), the formulation given in (1) by expressing a combined FM-AM signal in the time domain as follows:

$$s(t) = A_c(t) \cos[\theta_i(t)] \quad (12)$$

Substituting for $A_c(t)$ the Taylor expansion (8) and for $m(t)$ the expression given in (4), leads to:

$$A_c(t) = \sum_{k=0}^u \gamma_k \cos(k\omega_m t) \quad (13)$$

where u is the order of the polynomial (8) and the variables γ_k are linear combinations of the coefficients λ_k of that Taylor series. The general expression of the Fourier transform of a nonlinear AM-FM signal (12) becomes:

$$\begin{aligned} S(f) = & \frac{1}{4} \sum_{k=0}^u \gamma_k \sum_{\substack{\zeta_j = -\infty \\ j=1, \dots, v}}^{+\infty} \text{Re} \left\{ \prod_{i=1}^v \mathcal{J}_{\zeta_i}(\beta_i) \right\} \cdot \\ & \cdot \left\{ \delta \left[f - f_c^I - \left(\sum_{i=1}^v i\zeta_i + k \right) f_m \right] + \delta \left[f + f_c^I + \left(\sum_{i=1}^v i\zeta_i + k \right) f_m \right] + \right. \\ & \left. \delta \left[f - f_c^I - \left(\sum_{i=1}^v i\zeta_i - k \right) f_m \right] + \delta \left[f + f_c^I + \left(\sum_{i=1}^v i\zeta_i - k \right) f_m \right] \right\} \end{aligned} \quad (14)$$

Eq.(14), which represents the new formulation “NFAM” proposed in the present work, determines the structure of the frequency spectrum of a combined FM-AM signal having whatever nonlinear dependence in both frequency (7) and amplitude (8) as function of the modulating signal. It has to be stressed that the usage of Taylor series to express the nonlinear relationships among the characteristic parameters and the input signal should not be just considered as a mere mathematical simplification since it allows the derivation of an exact analytical solution even in the case in which these relationships exhibit nontrivial functional dependences.

The formulation (14) appears to be qualitatively similar to the relationship (11) as it predicts the same frequency shift of the carrier signal ($f_c - f_c^I$) together with the existence of symmetric sidebands having different amplitudes. Despite of this, it contains a quantitative difference with respect to (11). In fact, depending on the values of the coefficients γ_k , the two models might provide substantially different values for the amplitude of sidebands.

To test our model we take into account nonlinear dynamics occurring in magnetic oscillators subjected to the contemporary action of a *dc* and *ac* spin-polarized current. In particular, we analyze, by means of our own micromagnetic framework^{12-15,17}, magnetization dynamics occurring in the so-called magnetic nanocontact geometry^{6,8-11}, as the one depicted in Fig.1, whose details are given in “Methods”. We specifically examine whether the discussed “NFM” and “NFAM” models can predict, *quantitatively* and *contemporarily*, both the amount of the frequency shift of the carrier wave and the difference existing in the amplitude of the symmetrically located sidebands (features (i) and (ii) respectively, discussed previously).

Within our micromagnetic approach, the output signal is identified through the time-variations of the GMR signal¹⁸. It is assumed to be proportional to the angle of misalignment $\varphi(t)$ between the directions of the local magnetization vectors of the two ferromagnetic layers (see Fig.1) and, in first approximation, can be expressed as $g_{av}^*(t) = \left\langle (1 - \cos \varphi_k(t)) / 2 \right\rangle_{\text{contact}}$, where we average the local contributions $\varphi_k(t)$ over the contact area¹⁰⁻¹⁶. Results will demonstrate that such a simplistic assumption is enough accurate for the characterization of the observed nonlinear dynamics.

The numerical experiments consist of two stages, corresponding to the analysis without and with the modulating signal $m(t)$ respectively. During the first stage, we carry out the identification of the parameters which appear in the relationships among $f_i(t)$, $A_c(t)$ and $m(t)$ (eqs. (7) and (8)).

We consider thus a *dc* input bias current $I = I_{dc}$ to generate a stable microwave output signal^{8,10} that we associate to the carrier wave. Because no modulating signal has been considered, such

condition implies $g_{av}^*(t) = c(t)$. Based on the parameter set reported in “Methods”, we choose the value $I_{dc_0} = 18$ mA as the bias point which corresponds to the excitation of propagating spin-wave having frequency $f_c = 17.725$ GHz and amplitude $\lambda_0 = 0.34341$ (a.u.). In spite of our system exhibits a nonlinear behavior in a large interval of bias currents (we explored the range $13 \text{ mA} < I < 21 \text{ mA}$), we are interested in a small oscillations analysis around that bias point. To this aim, we sweep the current I in a restricted interval of currents under the constrain $|I - I_{dc_0}| < 1.5$ mA and report the corresponding values of f_i and A_c as in Fig.2. From these values, it is possible to approximate the nonlinear relationships $f_i(I)$ and $A_c(I)$ by computing analytically the Taylor series around the bias point: $f_i(I - I_{dc_0})$ and $A_c(I - I_{dc_0})$. Since the modulation process⁹, simulated during the second stage of the present analysis, is due to the superposition of a carrier wave and a modulating signal, the latter implemented as a sinusoidal *ac* current $I_{ac} = m(t) = A_m \cos(\omega_m t)$, the total bias current will be expressed as: $I = I_{dc_0} + m(t)$. Under these circumstances, the modulating signal is given by $m(t) = (I - I_{dc_0})$ and the previous Taylor expansions become explicitly dependent on the modulating signal, $f_i(m(t))$ and $A_c(m(t))$, under the constrain $A_m \ll I_{dc_0}$. This method allows the identification of the k_h and λ_k coefficients.

During the second stage of our approach, where the modulation process takes place, the output signal corresponds to the modulated signal, $g_{av}^*(t) = s(t)$, as defined in (1),(9) and (12). The analysis is performed by considering modulating signals having a fixed frequency $f_m = 500$ MHz and amplitude A_m which varies in the range $0 \div 1.5$ mA. For each value of A_m , we investigate the composition of the Fourier spectra, with particular emphasis to the amplitude and frequency of central peak, first-order and second-order sidebands.

Let us focus first on the relationship between the central frequency f_c^I and the amplitude of the modulating signal A_m (feature (i)). We compare the numerical results with those obtained

analytically by substituting the values of the coefficients k_h into eq.(10). Results of this comparison are shown in the main panel of Fig.3 and reveal a good agreement, as expected from the analogy with the approach carried out in Ref.9. We would like to notice that, since the even coefficients k_h are negative, the central frequency exhibits the expected red-frequency shift, *i.e.* f_c^I decreases with increasing the amplitude A_m . From this viewpoint, no differences are detected between results of model “NFM” and “NFAM”, in agreement with the theoretical prediction that the amplitude dependence (8) (*i.e.* the additive AM modulation process) does not shift the central frequency (10).

Let us focus now on the relationship between the amplitude of l th-order sidebands $|S(f = f_c^I \pm lf_m)|$ and the amplitude of the modulating signal A_m (feature (ii)). For simplicity, we limit our analysis to the study of first ($l=1$) and second ($l=2$) order sidebands. To summarize the investigated relationship in only one curve, we introduce a new dimensionless variable Ψ_l which represents the ratio between the amplitude of upper and lower sideband of l -th order: $\Psi_l = |S(f = f_c^I + lf_m)| / |S(f = f_c^I - lf_m)|$. If the modulated signal obtained by means of the described procedure were the result of a “pure” nonlinear FM process, as done in Ref.9, a substantial agreement between the numerical calculations and the theoretical results derived from the “NFM” model would be achieved. Results reveal, on the contrary, a remarkable disagreement between them (see Fig.4, dashed line).

This led us to investigate the origin of such discrepancy from both numerical and theoretical viewpoint. First, as observed in Fig.2 (dashed red curve), the output amplitude almost doubles its value when passing from $I = 16.5$ mA to $I = 19.5$ mA. It is a clear indication that the assumption $A_c = \text{constant}$ is inappropriate for this context and must be rejected. This is also the main reason why the approach carried out in Ref.9 could not accurately reproduce the different sidebands amplitudes. On the other hand, it has to be pointed out that the temporal evolution of microwave signals is not generally observable in experiments because of the limited bandwidth of measuring

instruments, and thus the estimation of the signal amplitude might be unfeasible. On the contrary, in this sense, a micromagnetic framework offers a powerful tool as it allows to handle an instrument having a theoretically infinite bandwidth. The feedbacks received from the numerical data processing reveal that the modulated signals present some characteristic features (mainly related to the envelope) ascribable to the simultaneous occurrence of an AM process (see insets in Fig.3). Second, a theory of microwave generation in current-driven magnetic oscillators demonstrated that the nonlinear shift of the generated frequency with the input current is strictly related to the variation of the projection of the magnetization vector on the precession axis which in turn demands for a change of the precession angle⁶. In fact, as discussed previously, any variation of the precession angle reflects, through the GMR effect, in a change of amplitude of the output signal. In other words, the relationship existing between the nonlinear frequency shift and the output amplitude cannot be disregarded. Analytical nonlinear dependences of both amplitude and frequency on the input bias current occurring in magnetic oscillators, like the ones here discussed, have been explicitly derived, for example, for both nanocontact^{6,19} and tunnel junction²⁰ geometry. All the above reasons yield us to include in our analysis also a nonlinear dependence of the output amplitude on the input bias current, as in eq.(8), and to develop a model for a combined FM-AM nonlinear modulator “NFAM”.

The result of the comparison between numerical calculations and theoretical ones (obtained by using eq.(14)) is shown in Fig.4 (solid line). The remarkable quantitative agreement, achieved without the usage of any adjustable parameter, confirms therefore the correctness of our conjecture about the simultaneous occurrence of two modulation processes stimulated by a sole input information-carrying signal. The above presented comparison of the analytical results arising from the generalized nonlinear model of a combined FM-AM modulation process with results of micromagnetic calculations performed on a magnetic nanocontact spin-transfer oscillator demonstrates that the “NFAM” model may give an accurate description of the complicate dynamics reported experimentally in Ref.9. The proposed approach might find application also in other

research fields, such as sonar communications, where an arbitrary chirp is modeled through a nonlinear combination of an AM and a PM signal (see Ref.21 and references thereafter). In those cases, both the amplitude and the phase of the modulated signal exhibits a very elaborated nonlinear dependence of time (see, *e.g.*, eqs.(4) and (8) of Ref.21) which generally prevents the derivation of an analytical solution for the corresponding integrals. By using our method, it would be possible, in principle, to overcome this difficulty and predict the composition of the frequency spectrum of the modulated signal.

METHODS

Here we report details on the implementation of the micromagnetic setup used to carry out the numerical experiments on the test case of a nonlinear magnetic nanocontact spintronic modulator.

A magnetic nanocontact device consists of a layered structure made by two extended magnetic layers (a thicker “fixed” or “pinned” layer (PL) and a thinner “free” layer (FL)) separated by a nonmagnetic spacer. A metallic circular contact of radius R_c is lithographically defined on the top of the FL, providing the opportunity to apply a perpendicular-to-plane current in a reduced region of the FL only (see Fig.1). The dynamics of the magnetization vector of the FL in both time and spatial domain, $\mathbf{M} = \mathbf{M}(t, \mathbf{r})$, is governed by the Landau-Lifshitz-Gilbert-Slonczewski (LLGS) equation:

$$\frac{\partial \mathbf{M}}{\partial t} = \gamma [\mathbf{H}_{\text{eff}} \times \mathbf{M}] + \frac{\alpha}{M_0} \left[\mathbf{M} \times \frac{\partial \mathbf{M}}{\partial t} \right] + f(r/R_c) \frac{\sigma I}{M_0} [\mathbf{M} \times (\mathbf{M} \times \mathbf{p})] \quad (15)$$

where γ is the gyromagnetic ratio and \mathbf{H}_{eff} is the effective magnetic field which includes magnetostatic, exchange, and Zeeman contributions. For simplicity, we neglect the current-induced (Oersted) magnetic field, the magnetostatic coupling between the two ferromagnetic layers and thermal fluctuations as they do not play a significant role in this context. We also ignore the magnetocrystalline anisotropy in the FL, which is an usual assumption for magnetically soft

Permalloy layers. The second term in the right-hand side of eq.(15) is the phenomenological magnetic damping torque written in the traditional Gilbert form (α is the damping constant) and $M_0 = |\mathbf{M}|$ is the saturation magnetization of the FL. The last term is the Slonczewski spin-transfer torque that is proportional to the bias current I . The function $f(r/R_c)$ describes the spatial distribution of the current across the area of the nanocontact. In the simplest case of uniform current density distribution, $f(r/R_c) = 1$ if $r < R_c$ and $f(r/R_c) = 0$ otherwise. The coefficient σ is related to the dimensionless spin polarization efficiency ε by $\sigma = \varepsilon g \mu_B / 2e M_0 S d_{FL}$, where g is the spectroscopic Landé factor, μ_B is the Bohr magneton, e is the absolute value of the electron charge, d_{FL} is the FL thickness and $S = \pi R_c^2$ is the nanocontact area. The unit vector \mathbf{p} defines the spin-polarization direction which coincides with the equilibrium direction of the PL magnetization. It is obtained by solving Brown's equation for the PL: $\mathbf{p} \times \mathbf{H}_{\text{eff}} = 0$ with no current.

In our approach, the LLGS equation is numerically solved by using our own three-dimensional (3D) finite-differences time-domain (FD-TD) micromagnetic code that employs a fifth-order Runge-Kutta integration scheme¹⁷.

The parameters used to simulate the current-induced spin-wave dynamics in a Permalloy FL are: thickness $d_{FL} = 5$ nm, nanocontact radius $R_c = 20$ nm, spin-polarization efficiency $\varepsilon = 0.25$, saturation magnetization $\mu_0 M_0 = 0.7$ T, spectroscopic Landé factor $g = 2.0$, and exchange stiffness constant $A_{FL} = 1.4 \times 10^{-11}$ J/m.

The magnitude $|\mathbf{H}_{\text{ext}}|$ of the external bias magnetic field is chosen to be $\mu_0 \mathbf{H}_{\text{ext}} = 0.8$ T and the field vector \mathbf{H}_{ext} is directed at 80 degrees out of the structure plane.

The parameters used to compute the equilibrium magnetic state of the Co-based PL are: thickness $d_{PL} = 20$ nm, saturation magnetization $\mu_0 P_0 = 1.88$ T and exchange stiffness constant $A_{PL} = 2.0 \times 10^{-11}$ J/m.

As discussed in previous works^{12-15,22-23}, in our numerical experiments we restrict our study to a limited square computational region as large as $L \times L \times d_{FL} = 800 \times 800 \times 5 \text{ nm}^3$, by using a 2D mesh of discretization cells having sizes $4 \times 4 \times 5 \text{ nm}^3$. To avoid the spurious spin-wave reflection from the computational boundaries we implement abrupt absorbing boundary conditions, as in Refs.12-13. Compatibly with a reasonable computational time, each simulation is long enough to assure a spectral accuracy as fine as 0.5 MHz.

As a result of the identification phase described in the main text, we get a fourth-order polynomial, as in eq.(7), for the expression $f_i(m(t))$ with coefficients: $k_1 = 0.15500 \text{ GHz/mA}$, $k_2 = -0.01300 \text{ GHz/mA}^2$, $k_3 = 0.00883 \text{ GHz/mA}^3$, $k_4 = -0.00160 \text{ GHz/mA}^4$ (Fig.2, black solid line). Analogously, the best fit which represents the function $A_c(m(t))$ is expressed in the form of a third-order polynomial, as in (8), with coefficients: $\lambda_0 = 0.34341$, $\lambda_1 = 0.05350 \text{ mA}^{-1}$, $\lambda_2 = -0.01400 \text{ mA}^{-2}$, $\lambda_3 = 0.0007 \text{ mA}^{-3}$ (Fig.2, dashed red curve). It has to be mentioned that, from the experimental point of view, it should be possible, at least in principle, to measure the sensitivity coefficients k_h and λ_k by using, for example, a generalization to the nonlinear case of the techniques proposed in Refs.2,24-25.

Acknowledgments

This research was supported by the Spanish government (project MAT2008-04706/NAN), by the Junta de Castilla y Leon (project SA025A08) and by Consorzio Interuniversitario di Scienze Fisiche della Materia (CNISM) (Progetto Innesco).

REFERENCES

- [1]. Haykin, S. *Communication systems* (John Wiley and Sons, 5th edition, 2009).

- [2]. Safronov, G.S. and Yatsenko, A.P. Measurement of the modulation factor of amplitude-phase-frequency modulated oscillations. *Measurement Techniques* **10**, 1494-1496 (1967).
- [3]. Stoker, J. J. Nonlinear Vibrations in Mechanical and Electrical Systems (Interscience Publishers, New York, 1950).
- [4]. Milotti, E. Nonlinear behaviour in a torsion pendulum. *Eur. J. Phys.* **22**, 239-248 (2001).
- [5]. He, J.H. Solution of nonlinear equations by ancient Chinese algorithm. *Applied Mathematics and Computation* **151**, 293-297 (2004). represent
- [6]. Slavin, A.N. and Kabos, P. Approximate Theory of Microwave Generation in a Current-Driven Magnetic Nanocontact Magnetized in an Arbitrary Direction. *IEEE Trans. Magn.* **41**, 1264-1273 (2005).
- [7]. Slonczewski, J.C. Current-driven excitation of magnetic multilayers. *J. Magn. Magn. Mater.* **159**, L1–L7 (1996).
- [8]. Slonczewski, J.C. Excitation of spin waves by an electric current. *J. Magn. Magn. Mater.* **195**, L261–L268 (1999).
- [9]. Pufall, M.R. et al., Frequency modulation of spin-transfer oscillators. *Appl. Phys. Lett.* **86**, 082506 (2005).
- [10]. Rippard, W.H. et al., Direct-Current Induced Dynamics in Co₉₀Fe₁₀/Ni₈₀Fe₂₀ Point Contacts. *Phys. Rev. Lett.* **92**, 027201 (2004).
- [11]. Rippard, W.H. et al., Current-driven microwave dynamics in magnetic point contacts as a function of applied field angle. *Phys. Rev. B* **70**, 100406(R) (2004).
- [12]. Consolo, G. Lopez-Diaz, L. Torres, L. and Azzerboni, B. Magnetization dynamics in nanocontact current controlled oscillators. *Phys. Rev. B* **75**, 214428 (2007).
- [13]. Consolo, G. Lopez-Diaz, L. Torres, L. and Azzerboni, B. Boundary Conditions for Spin-Wave Absorption Based on Different Site-Dependent Damping Functions. *IEEE Trans. Magn.* **43**, 2974-2976 (2007).

- [14]. Consolo, G. et al. Excitation of self-localized spin-wave bullets by spin-polarized current in in-plane magnetized magnetic nanocontacts: A micromagnetic study. *Phys. Rev. B* **76**, 144410 (2007).
- [15]. Consolo, G. et al. Micromagnetic study of the above-threshold generation regime in a spin-torque oscillator based on a magnetic nanocontact magnetized at an arbitrary angle. *Phys. Rev. B* **78**, 014420 (2008). Succeed
- [16]. Kiselev, S.I. et al. Microwave oscillations of a nanomagnet driven by a spin-polarized current. *Nature* **425**, 380-383 (2003).
- [17]. Romeo, A. et al. A numerical solution of the magnetization reversal modeling in a permalloy thin film using fifth order Runge–Kutta method with adaptive step size control. *Physica B* **403**, 464-468 (2008).
- [18]. Baibich, M.N. et al. Giant Magnetoresistance of (001)Fe/(001)Cr Magnetic Superlattices. *Phys. Rev. Lett.* **61**, 2472-2475 (1988).
- [19]. A. Slavin and V. Tiberkevich, Excitation of Spin Waves by Spin-Polarized Current in Magnetic Nano-Structures. *IEEE Trans. Magn.* **44**, 1916-1927 (2008).
- [20]. Deac, A.M. et al. Bias-driven high-power microwave emission from MgO-based tunnel magnetoresistance devices. *Nature Physics* **4**, 803-809 (2008).
- [21]. Collins, T and Atkins, P. Nonlinear frequency modulation chirps for active sonar. *IEEE Proc. Radar, Sonar Navig.* **146**, 312-316 (1999).
- [22]. Berkov, D.V. and Gorn, N.L. Micromagnetic simulations of the magnetization precession induced by a spin-polarized current in a point-contact geometry. *J. Appl. Phys.* **99**, 08Q701 (2006).
- [23]. Berkov, D.V. and Miltat, J. Spin-torque driven magnetization dynamics: Micromagnetic Modeling. *J. Magn. Magn. Mater.* **320**, 1238-1259 (2008).
- [24]. Ya. Sup'yan, V. Measurement of the parameters of phase-modulated oscillations. *Measurement Techniques* **6**, 769-771 (1963).

- [25]. Grigorev, V.A. and Dorokhov, A.N. Spectral measurement of frequency modulation index. *Measurement Techniques* **41**, 842-847 (1998).

Figures

Fig.1

Schematics of a magnetic multilayer nanocontact device. It consists of two extended ferromagnetic layers (a thicker “Pinned Layer” (PL) and a thinner “Free Layer” (FL)) separated by a non-magnetic spacer. Lateral dimensions in the order of micron are experimentally employed for this class of device to reduce the effects of edge roughness and defects. In this sense, the magnetic layers can be treated as they were not bounded in the plane. A lithographically defined contact is made on the top of the FL, providing the opportunity to apply a perpendicular-to-plane bias current only in a reduced region of the device. A current flowing from the PL to the FL, having intensity above a given threshold, acts as a perturbation of the equilibrium magnetic state. The device is also biased by an external static magnetic field. Because of the action of such field, and of the larger volume and saturation magnetization of the PL with respect to the FL, magnetization dynamics occurring in the PL are safely neglected. Only current-induced magnetization dynamics in the FL are thus considered.

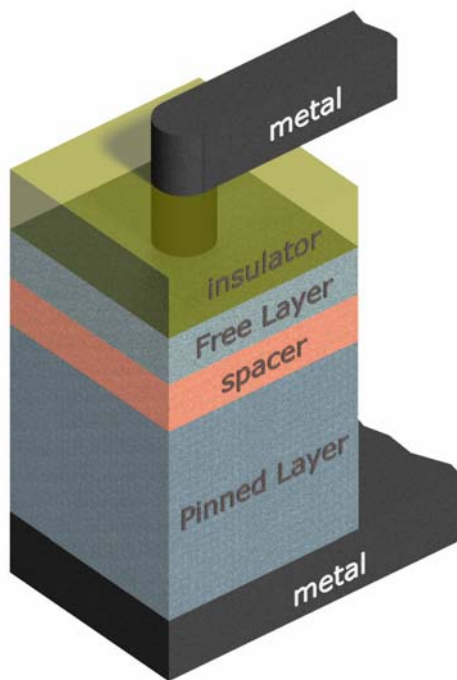


Fig.2

Dependence of frequency f_i (black symbols) and amplitude A_c (red symbols) on the input current I_{dc} . The corresponding polynomial fits are shown by the solid black curve (eq.(7)) and the dashed red curve (eq.(8)) respectively.

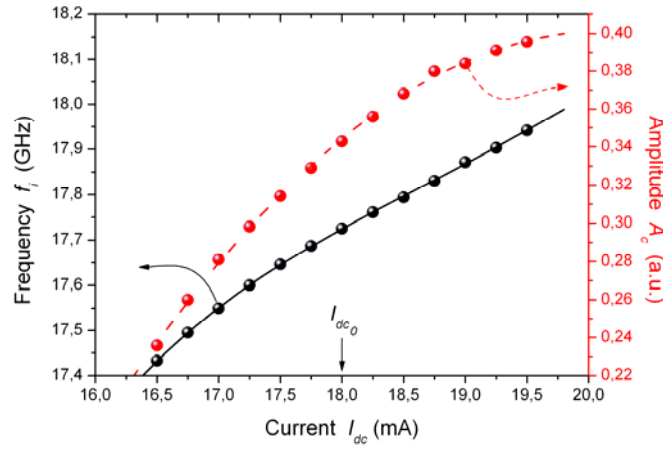


Fig.3

Main panel: dependence of the central frequency f_c^I on the amplitude of the modulating signal A_m . Symbols are representative of numerical results whereas solid line shows the theoretical dependence predicted by both NFM and NFAM model.

Insets: Details of the temporal evolution of the modulated signal $g_{av}^*(t)$ for $A_m = 0.125$ mA (bottom left figure) and $A_m = 1.5$ mA (top right figure).

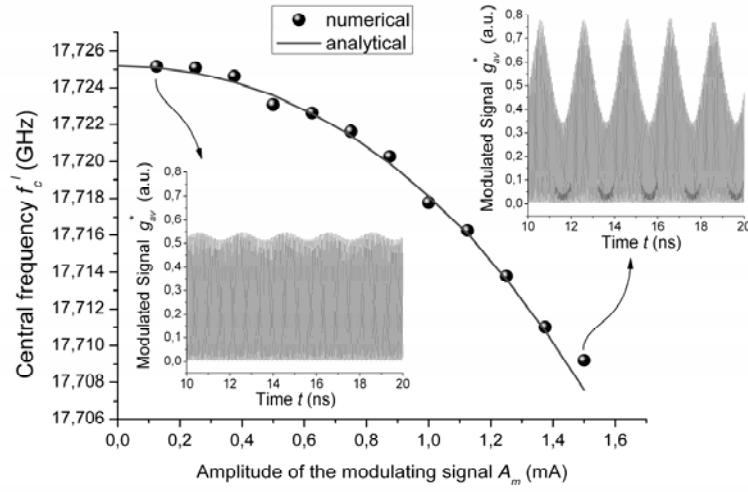


Fig.4

Dependence of (a) 1st-order and (b) 2nd-order sidebands amplitude ratio on the amplitude of the modulating signal. Symbols, together with error bars, are representative of numerical results, whereas the analytical ones are denoted by lines (dashed line for NFM and solid line for NFAM). Error bars associated to numerical results are representative of a computational error of about 2.5%.

